ETH
Eidgenössische Technische Hochschule Zürich
Swiss Federal Institute of Technology Zurich

PAUL SCHERRER INSTITUT
PSI

Implementation of a continuous phase-stepping CT data acquisition and analysis pipeline

Semester Thesis

Ketan Gupta

June 17, 2022

Supervisor: Prof. Dr. M. Stampanoni

Advisor: S. Spindler

Department of Information Technology and Electrical Engineering, ETH Zürich

Abstract

This project seeked to evaluate the validity of continuous phase stepping for acquiring images with Talbot-Lau interferometry. Differential phase contrast computed tomography with continuous phase stepping yielded comparable results to discrete phase stepping. An imaging pipeline was developed that could acquire data over a desired period for continuous stepping. The periodicity of the phase stepping has been evaluated over the whole piezo range to calibrate further measurements.

Acknowledgement

Contents

Chapter 1

Introduction

Ever since X-rays were discovered in the late 19th Century, they have been used in a wide variety of ways. One area in which they have proved especially useful is in projection imaging through the volume of materials due to their highly penetrative capabilities. X-rays are a type of electromagnetic radiation that have wavelengths ranging from 0.01 nm to 10 nm [1][Ch. 7]. X-rays can penetrate through biological tissue, which makes them useful for medical imaging and radiotherapy.

1.1 X-ray generation, interactions with matter and the simplest X-ray images

The oldest, but still used, method for X-ray generation is the X-ray tube; today, these are the primarily used radiation sources for medical imaging, due to them being relatively inexpensive. A negatively charged filament, or cathode, is heated in order to induce emission of electrons. An anode, typically made of tungsten, is given a positive charge. The voltage difference between the anode and cathode accelerates the electrons towards the anode. As the electrons strike the anode, X-ray generation occurs via two mechanisms: characteristic radiation and Bremmstrahlung [1][Ch. 7]. Characteristic radiation occurs when an emitted electron knocks an electron from an inner shell of an atom in the anode out of its orbit. An outer shell electron moves down energy levels to fill this hole, and in so doing releases a photon, the energy of which is specific to the differences in energy levels of the anode element. During Bremmstrahlung, an electron emitted from the cathode will decelerate and its trajectory will be altered as it passes close to an atom in the anode. This causes the emission of photons, the energy of which is a continuous spectrum [1][Ch. 7].
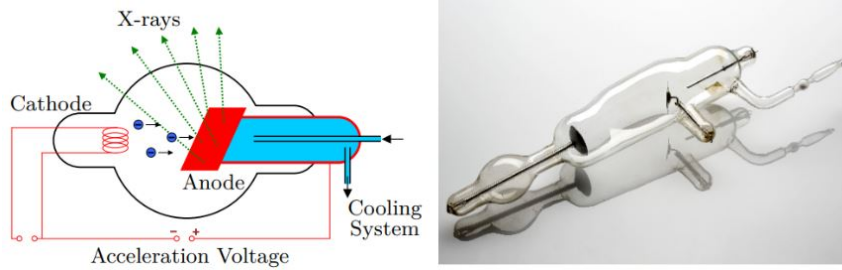
Figure 1.1: On the left, a schematic of an X-ray tube. On the right, a historic vacuum X-ray tube. Images taken from [1][Ch. 7].

When X-rays coming out of a tube travel through matter, they undergo a phase shift and a decrease in intensity - or attenuation - due to the material's refractive index. For X-ray photon energies, the complex index of refraction for a medium can be expressed as [1][Ch. 9]

$$n = 1 - \delta + i\beta \tag{1.1}$$

δ contains the phase information and β contains the attenuation information. The degree of attenuation depends on the attenuation coefficient of materials in the beam path, which is medium-dependent, as well as the distance traveled through a given sample. The mathematical formula that governs this drop in intensity is the Beer-Lambert Law [1][Ch. 7]:

$$I = \int_0^{E_{max}} I_o(E) e^{-\int \mu(x,E)\,dx} \; dE \tag{1.2}$$

In Eq. 1.2, I_o is the initial intensity of each photon energy, x is the position in the sample, μ is the attenuation coefficient (which is photon energy dependent) at x and E is the photon energy. This equation involves an integration over photon energy when the illumination is polychromatic.

X-rays are useful for imaging, owing to their high penetrability due to their high frequencies. In projection, or absorption images, a film or detector array is placed behind the sample. Before imaging a sample, a flat-field measurement is necessary. This is a map of the X-ray intensities that strike the detector with no sample present. A projection image is produced by comparing the intensity recorded when a sample is present with the flat-field measurement. The intensity of the sample image is given by the Beer-Lambert Law (Eq. 1.2), with I_o being the flat-field intensity. This method of imaging is called radiography, and is most commonly used in order to image patients' bones. Images of bones achieve good contrast due to the fact that

bones and soft tissue have significantly different attenuation coefficients; for example, at a photon energy of 30 keV, bone's attenuation coefficient is 2.556 cm^{-1} [2] and soft tissue's (ICRU-44) attenuation coefficient is 0.402 cm^{-1} [2]. A drawback of this imaging modality is that it does not produce good contrast for materials with attenuation coefficients that are close in value; breast tissue's attenuation coefficient is 0.347 cm^{-1} [2], which is comparable to ICRU-44. This makes absorption imaging unsuited to applications that require imaging of different types of soft tissues.

Figure 1.2: On the left, radiographic images of an arm with fractures. On the right, metal rods used to fix the fractures. Images taken from [1][Ch. 7].

In order to image different types of soft tissue, the phase shift can be exploited. δ for X-rays is typically higher than β by a factor of 1000 [1][Ch. 9]. In theory, it should be possible to get from δ a signal that is 1000x stronger than an attenuation-based image. One approach that enables the retrieval of phase information is Talbot-Lau Interferometry.

1.2 Talbot-Lau Interferometry (TLI)
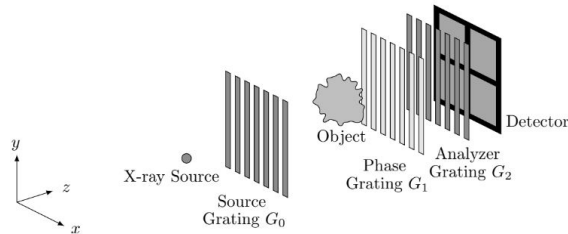
Figure 1.3: A schematic of a Talbot-Lau interferometer. The setup used for this report had the object be positioned downstream of G1, rather than upstream as shown here. Image taken from [1][Ch. 9].

Talbot-Lau interferometry relies on the interference properties of electromagnetic waves. G0 is an absorption grating i.e. its bars strongly attenuate light incident on them. G1 is a phase grating i.e. its bars cause a phase shift in light that passes through them. This allows constructive or destructive interference to occur between light rays that pass between a slit or bar of G1. Due to the Talbot effect, a Talbot carpet is formed downstream of G1. At periodic distance intervals, an interference profile with a clearly distinguishable black-and-white pattern is formed. G2 is placed at one of these distance intervals.
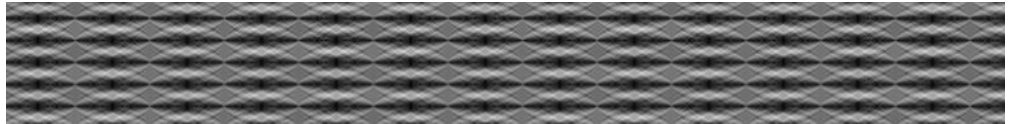
Figure 1.4: A simulated Talbot carpet. The beam moves from left to right. Image taken from [1][Ch. 9].

Akin to how in Young's experiment a pinhole was used to produce coherent light, the grating G0 serves as an array of pinholes; coherent light is required in order to produce the interference effects that are used to get TLI readings. Using a grating rather than a pinhole allows a greater photon flux to progress towards the sample. This produces a stronger signal than a pinhole and allows the X-ray source to be used more efficiently.

G2 is called the analyzer grating and like G0 is an absorption grating. This is present immediately upstream of the detector. The detector's pixels are larger than the width of the interference pattern's period, which is why G2 is used to resolve the pattern via a process called phase stepping.
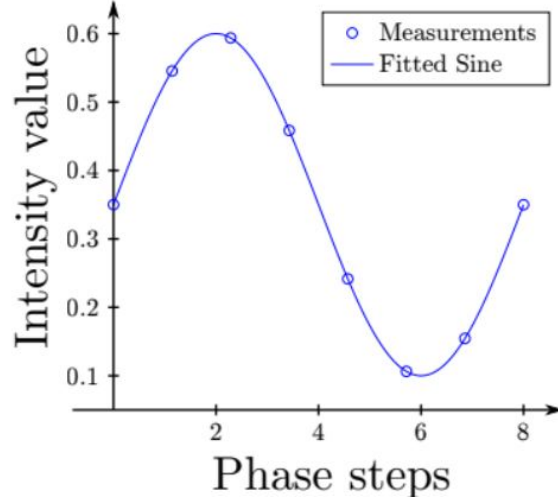
Figure 1.5: An example of a phase stepping curve with a fitted sinusoid. Image taken from [1][Ch. 9].

As shown in Fig. 1.4, the intensity readings for each phase step can be fitted to a sinusoidal function. This sinusoid is applied to each detector pixel in a process called signal retrieval and is modeled by:

$$I_{fit}(x) = I_{measured} \left[0.5 V_{measured} \times \cos \left(\frac{2\pi}{period} x + \varphi \right) + 0.5 \right] \qquad (1.3)$$

x in Eq. 1.3 denotes the phase steps, V denotes the visibility (covered in Eq. 1.6) and φ denotes the phase. The fitted sinusoid has three useful properties: an offset, amplitude and phase. In order to produce useful TLI data, a phase stepped flat-field measurement is required. Using the sinusoidal fits for the sample and flat-field measurements, three values can be obtained as the result of TLI: attenuation, phase and dark field. Attenuation is essentially a comparison of the mean or offset values of the sinusoidal curves, and is given by [1][Ch. 9]:

$$\mu = -ln \left(\frac{\sum_{i=1}^{n} R_i}{\sum_{i=1}^{n} O_i} \right) \qquad (1.4)$$

In Eq. 1.4, R denotes the fit for the phase stepping measurements of the flat-field - or reference - and O denotes the fit for the measurements of the sample - or object. n is the total number of phase steps. The phase can be found by calculating the phase shift of the sample measurement relative to the flat field:

$$\varphi_{shift} = \varphi_R - \varphi_O \qquad (1.5)$$

The dark field signal (D) is a function of the visibilities of the flat-field V_R and of the sample object V_O [1][Ch. 9]:

$$V_R = \frac{max(R) - min(R)}{max(R) + min(R)} \qquad (1.6)$$

$$D = -ln\left(\frac{V_R}{V_O}\right) \qquad (1.7)$$

Attenuation images can help distinguish attenuating macroscopic features from a background but do not achieve high contrast between fine details. Phase contrast images contain more information on high spatial frequency details such as edges [1][Ch. 9]. Dark field signals are sensitive to scattering in the sample; such images can contain fine details that attenuation cannot.

1.3 Computed Tomography (CT)

A drawback of projection images is that the recorded intensity at each pixel represents the combined effects of all the various attenuation coefficients along the beam path i.e. a line integral of the attenuation coefficients which is given by the Beer-Lambert Law (Eq. 1.2). In order to calculate the coefficients, and to therefore find the spatial make up of a sample, computed tomography can be used. Unlike projection images (Fig. 1.5), CT can find spatially specific information across three-dimensional slices. CT involves taking projection images from a range of angles in order to find out how different substances in a sample are spatially arranged. An example of an instance in which this method is useful is taking images of lungs, which may be obstructed by ribs. If a projection image was taken, the attenuation by the ribs would be too strong and no soft lung tissue would be visible. By performing a tomographic image, one could recover the tissues contained within a slice of interest. Computed tomography relies on a few key principles, the first of which is the Radon Transform [1][Ch. 8]:

$$p(\theta, s) = \int\int_{-\infty}^{\infty} f(x,y)\delta(xcos\theta + ysin\theta - s)dxdy \qquad (1.8)$$

The Radon Transform shows that any integrable function of interest $f(x,y)$ can be represented by line integrals over that function's domain. In Eq. , the line is given by $s = xcos\theta + ysin\theta$. The Dirac delta function selects only those x and y values that lie on the respective line. By going from $\theta = [0, \pi]$ and

$s = (-\infty, \infty)$, the complete set of line integrals can be retrieved uniquely. In the context of CT imaging, Radon transforms are performed by measuring the projection of the sample at different angles (θ) and stacking these with respect to the angle. The result of this is called a sinogram, as the curves look sinusoidal. The Radon Transform is the process of converting a function $f(x, y)$ to its line integral values with respect to angle. Since measurements taken downstream of the sample are projections, the intensities of which depend on the attenuation coefficients present in the beam path, $f(x, y)$ can be thought of as a spatial map of the sample's attenuation coefficients. To find this is the goal of CT.
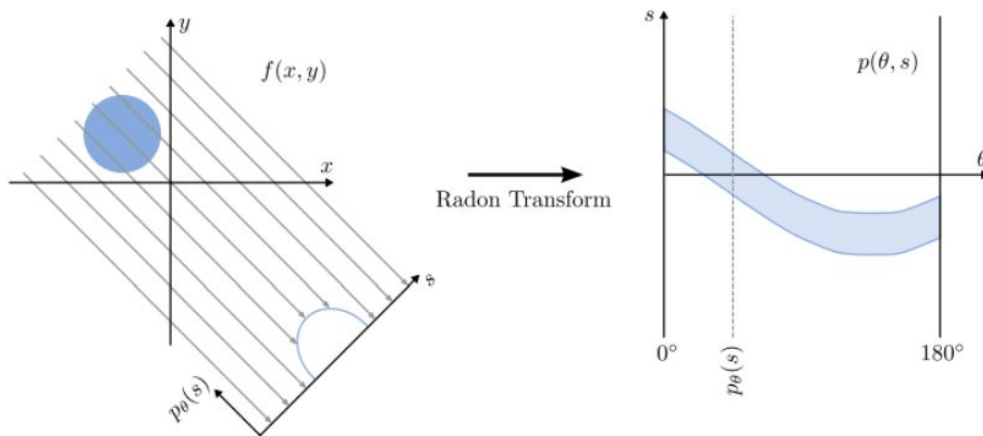
Figure 1.6: The sample being measured (left) and the sinogram resulting from its Radon transform (right). Image taken from [1][Ch. 8].

The next important concept for CT is the Fourier Slice Theorem. According to the Fourier Slice Theorem, if the 2D Fourier transform of f along a straight line passing through the origin along an angle θ is taken, one will retrieve the Fourier transform of the projection of the sample taken at the angle θ. In effect, it is possible to find the Fourier transform of the unknown function $f(x, y)$ by sampling the Radon transform (the projections) in Fourier space along lines of different angles.

7
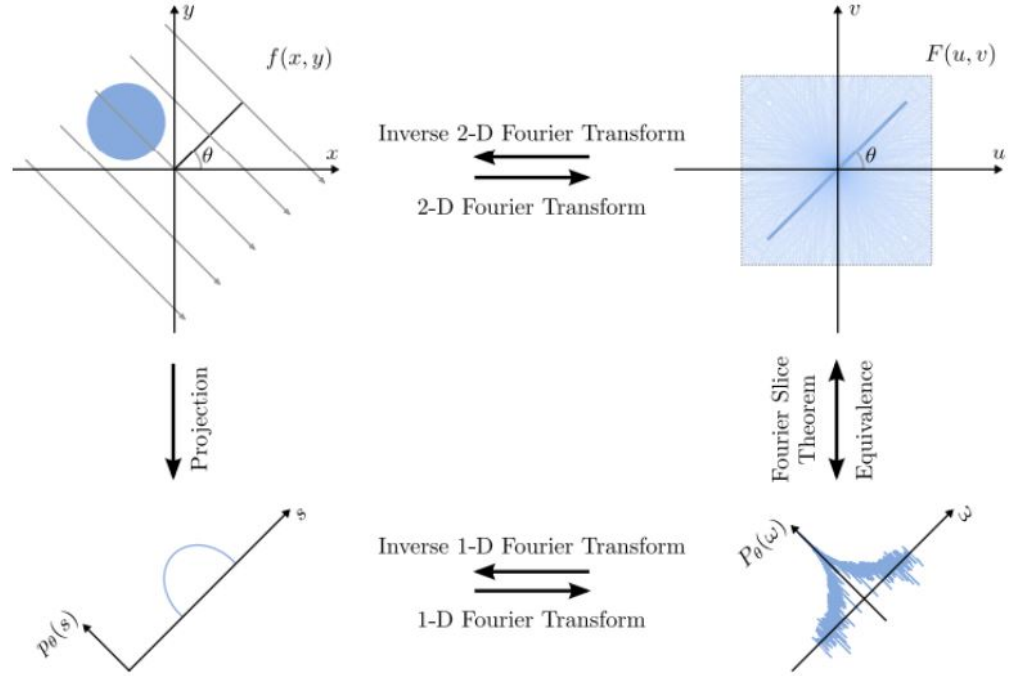
Figure 1.7: An illustration of the Fourier Slice Theorem, taken from [1][Ch. 8].

If we know the Radon transform of $f(x, y)$, which is physically obtained as a sinogram, we can find f. This is done by multiplying the Fourier transform of Eq. 1.8 with a filter in the Fourier space, and then performing an inverse Fast Fourier Transform on the multiplication's result. One such filter is $|\xi|$ where ξ is the spatial frequency. Sampling radially results in a greater density of samples in the near-zero frequencies. Less higher frequency information results in a lower resolution. Using this filter ensures that high frequency information is represented in the final result. Other filters may also be used; at high frequencies data is noisier, so there may be the need for a filter that tapers off at high frequencies [1][Ch. 8].

$$f(x,y) = \int_0^\pi \int_{-\infty}^\infty P(\xi,\theta)|\xi|e^{2\pi i \xi s} d\xi d\theta \tag{1.9}$$

The process of going from the Fourier transform ($P(\xi, \theta)$) of the sample projections to a spatial map $f(x, y)$ of the sample's attenuation coefficients is known as Filtered Backpropagation (Eq. 1.9). A special type of filter known as a Hilbert filter [1][Ch. 9] can be used to find the δ, or phase shift, of different media in a sample.

For each projection angle, signal retrieval can be performed. The signal retrieved data, after flat field correction, can then be reconstructed through CT in order to yield three tomographic images; these are spatial maps of the attenuation, phase shift and dark field.

1.4 Aim of Thesis

The goal of this semester project was to show that phase stepping measurements can be obtained using continuous movement of the phase stepping grating. A working acquisition script would be developed in order to implement this on a Talbot-Lau interferometer prototype operated by Prof. Stampanoni's group at the Paul Scherrer Institute. Motion profiles suited to continuous movement would need to be implemented and an analysis pipeline to handle signal retrieval would also be developed. Data would be reconstructed and compared to discrete (stop-and-shoot) phase stepping. An imaging protocol to acquire data for continuous phase stepping of a desired period would be developed. With a view to future fast stepping applications, the periodicity of phase stepping curves would be evaluated for different G0 positions and types of phase stepping.

Chapter 2

Setup

Prof. Stampanoni's group at the Paul Scherrer Institute operates Talbot-Lau interferometer prototypes. All experiments were performed on a modular setup which allowed for the efficient alteration of parts and geometries.
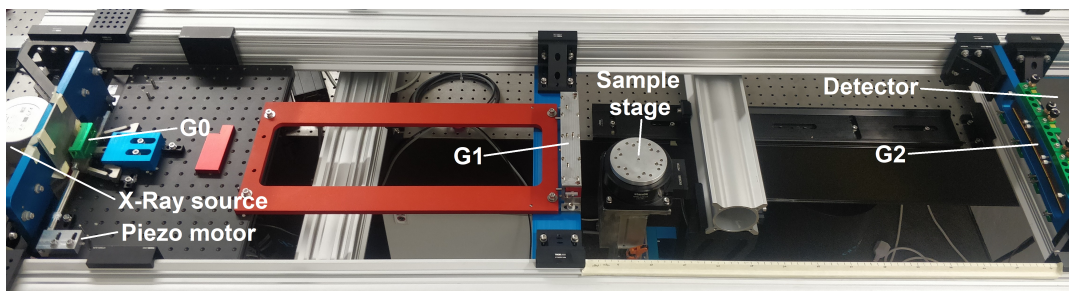
Figure 2.1: A picture of the setup used for the experiments

2.1 Components

X-ray source: The radiation source used was the X-ray tube Comet MXR-225HP/11 with a conical beam. An aluminum plate was used as a high pass filter for the light.

Gratings: As per Section 1.2, three gratings - named G0, G1 and G2 - were used in order to perform Talbot-Lau interferometry. G0 served as the absorption grating in order to create an array of spatially coherent light sources and was placed directly downstream of the tube. G0's other key function was to be translated perpendicular to the beam path to achieve phase stepping. G1 was a phase grating placed immediately upstream of the sample and its function was to produce a Talbot carpet. Like G0, G2 was an absorption grating. It was placed immediately upstream of the detector and served as the analyzer grating. All gratings had a duty cycle of 0.5.

Phase stepping: Translation of G0 perpendicular to the beam path for phase stepping was executed by a P-841.60 piezo motor and an E-709 piezo driver manufactured by Physik Instrumente. The driver was instructed using Python; the modules used were *GCSDevice* [3] and *pitools* [3] from the *pipython* [3] library.

Sample: The sample was placed between G1 and G2. It was placed on a stage which could be vertically translated as well as rotated. Rotation was used to acquire tomographies.

Detector: A Dectris Titlis T02402 75-0 detector was used to acquire images. This was a 2D array of detector pixels. Cadmium telluride crystals were used.

2.2 Piezo driver modes for continuous phase stepping

To achieve continuous phase stepping, modes were used that would move G0 in a linear fashion. These modes are called wavetables, and are predetermined trajectories that the piezo driver would always execute to completion. During the execution of the linear wavetables, G0 would first accelerate, then move linearly and then decelerate.

The wavetable executed can be divided into some number of table points; this number was 2000 for the wavetables used in this report. For each point, the driver would refresh depending on a servo update time in order to ensure that the piezo motor's position was where it should be. This update time was 0.1 ms [4].
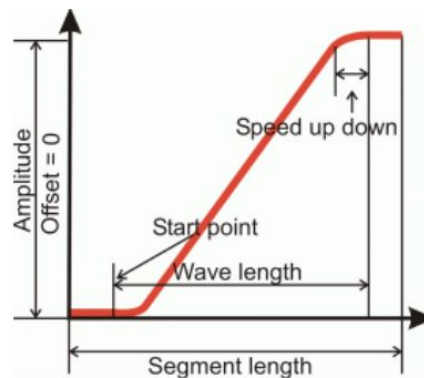
Figure 2.2: A general plot of the linear wavetables used for continuous phase stepping. The y-axis represents the displacement of the piezo motor from its rest position, and the x-axis represents time. This figure was taken from the instruction manual for the E-709 piezo driver by Physik Instrumente [4].

Wavetable number	Amplitude [μm]	Tablepoints
1	4.51	2000
2	20	2000

Table 2.1: Details of wavetables used [4].

2.3   Signal retrieval

The signal retrieval would fit a sinusoidal function - given by Eq. 1.3 - to the phase stepping data. For each pixel, the recorded intensities corresponding to each phase step would be signal retrieved. The period calculation would involve testing different test period values within a bracketing interval; the period that yielded the least squares difference of the sinusoid compared to the data would be the period returned. After flat-field and sample measurements were acquired with a known period in mind, a sinusoidal function with this period would be fitted to the data prior to flat-field correction.

2.4   Rotational motor for CT

The motor that rotated the sample for the purpose of varying angular projection images was limited in that it could only execute a constant rotational speed of integer RPMs. In order to perform tomographic images at slower speeds, the motor was controlled such that it took small steps at a high frequency.

Chapter 3

Computed Tomography for Discrete and Continuous Phase Stepping

To show that continuous phase stepping is feasible, it was necessary to acquire images with discrete and continuous phase stepping. These images would then be compared through a quantitative metric: the contrast-to-noise ratio (CNR, described in Section 3.3). The benefit of performing continuous phase stepping would be reduced acquisition times compared to discrete stepping. Whereas for the former where G0 is constantly moving, in the latter image acquisition must be halted while G0 is stepped to its next position.

In order to compare discrete and continuous phase stepping, four tomographic image sets of a phantom were acquired and then compared via their CNRs. For each image acquired, two flats were acquired for the purposes of flat-field correction. A flat-field measurement would be taken prior to and after the main sample measurement. The two flat-field measurements would then be averaged and signal retrieved. Performing this correction ensured that the final image would be free from noise such as from the phase drift from the X-ray source.

The total exposure time was a control variable, and the exposure time chosen for each image was 25 minutes. Discrete and continuous phase stepping images were acquired at two rotational speeds, 0.2 and 1 RPM.

3.1 Discrete phase stepping

5 phase steps were used for these measurements. For data acquisition during each phase step, G0 would be stationary. After the respective projections were acquired, the piezo motor would then move G0 a distance equal to $1/5^{th}$ of the pre-calculated G0 period to reach the next phase step.

Before the acquisition of the complete discrete phase stepping tomography,

a short flat-field measurement was performed (exposure time = 20 s). After retrieving the signal, the optimal period for G0 would be calculated and then used for the acquisition detailed below.

Over the course of the measurement with slow rotation (0.2 RPM) of the sample, the sample would complete 5 rotations over the course of the exposure time, and one tomographic image would be acquired for the entire duration. After each 360° rotation of the sample, G0 would be moved to the next phase step. The benefit of slow rotation is that each projection angle of the sample would yield frames with higher statistics.

For fast rotation of the sample at 1 RPM, the sample would complete 25 rotations. For each subdivision of 5 rotations, one complete phase stepping image would be taken; G0 would be stepped after each 360° rotation. After performing flat-field correction, the five images would be averaged before tomographic reconstruction. Acquiring 5 images meant that the statistics of this measurement could be compared to the slow rotation's data.
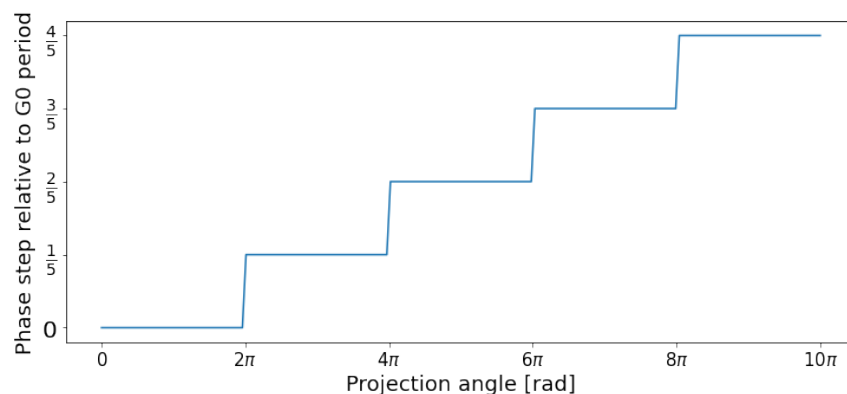
Figure 3.1: The stepping and sample rotation protocol used for a rotation speed of 0.2 RPM.
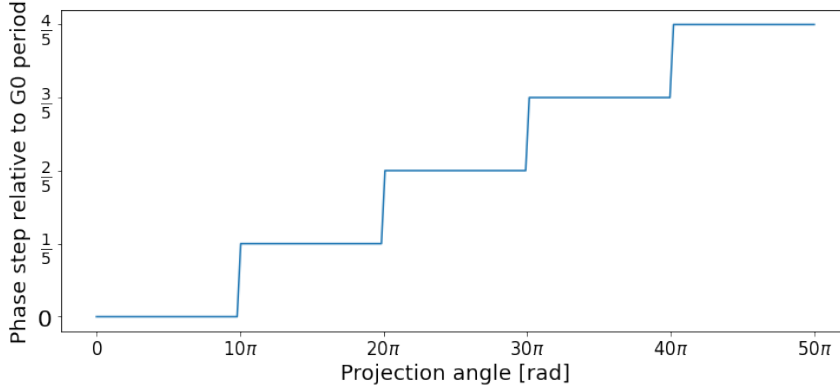
Figure 3.2: The stepping and sample rotation protocol used for a rotation speed of 1 RPM.

In post-processing, the frames acquired during the piezo move time between phase steps were removed before analysis. The number of frames removed equaled the piezo move time multiplied by the detector frame rate. This frame removal was performed after increments representing each complete set of angular projections for each phase step.

3.2 Continuous phase stepping

This involved using a continuous movement profile of the piezo driver, also known as a wavetable (described in Section 2.3), during data acquisition. Wavetable 1 was used for these measurements. The amplitude, or ending location of the wavetable and therefore G0, was a fixed value of 4.51 um. Unlike for discrete phase stepping, no frame removal due to piezo motion between phase steps is required. Similar to discrete phase stepping, flat-field measurements were taken prior to and after the main sample image.

For the slow rotation measurement at 0.2 RPM, the sample would complete 5 rotations over the course of the exposure time (25 mins), and one image would be acquired for the entire duration. Over this duration, the piezo driver would execute the wavetable once. Thus, for each rotation, the data acquired would correspond to $1/5^{th}$ of 4.51 um. During each rotation, as the angle of rotation increased from 0 to 360°, there was a linearly increasing phase shift due to the continuous motion of G0. This shift needed to be subtracted from the flat-field corrected signal prior to reconstruction. If N_{proj} projections were taken and the period calculated from the retrieved signal was $p_{G0,calculated}$ with n_i being the index of a particular projection, then the corresponding phase shift for that projection is given by:

$$\Delta_{phase\,shift,i} = \frac{2\pi \times n_i}{N_{proj}} \times \frac{Wavetable\;amplitude}{p_{G0,calculated}}$$

(3.1)

During the fast rotation measurement at 1 RPM, The sample would complete 25 rotations. Each subdivision of 5 rotations would correspond to a G0 movement equaling $1/5^{th}$ of 4.51 um. Each 360° rotation corresponded to $1/25^{th}$ of G0's assumed period. Thus, there are 25 phase steps for continuous phase stepping at 1 RPM, as opposed to 5 phase steps for discrete phase stepping. After performing flat-field correction, the five images would be averaged before tomographic reconstruction. Similar to the slow rotation, there was a linearly increasing phase shift for each projection angle which needed to be subtracted prior to reconstruction. This is also governed by Eq. 3.1.

3.3 Data and CNR calculation

CT reconstructions were performed using the ASTRA-Toolbox [5].
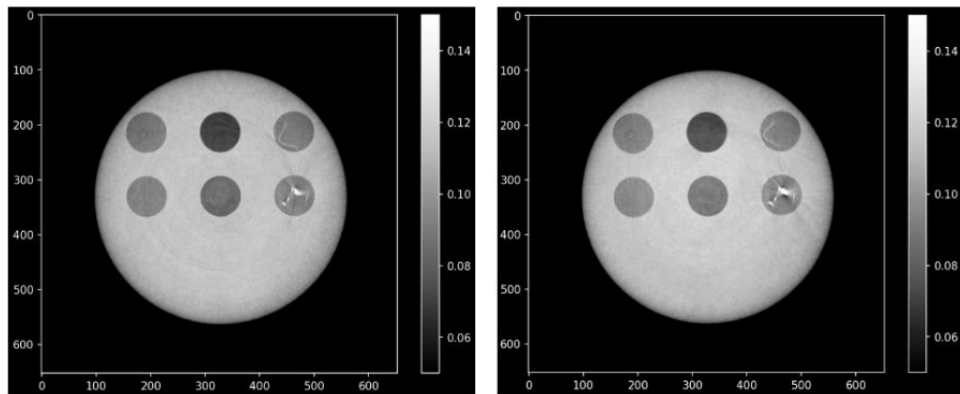
Figure 3.3: Tomographic phase contrast reconstruction of phantom acquired with slow rotation at 0.2 RPM. Left: discrete phase stepping. Right: continuous phase stepping.
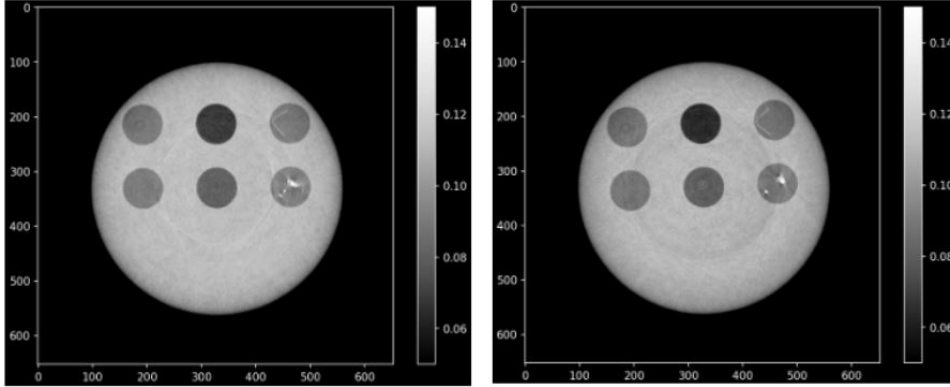
Figure 3.4: Tomographic phase contrast reconstruction of phantom acquired with fast rotation at 1 RPM. Left: discrete phase stepping. Right: continuous phase stepping.

The performance of each acquisition mode was evaluated by calculating the contrast to noise ratio (CNR) for the phase contrast images. The CNR was calculated for various patches in the phantom, which correspond to different materials. The patches were chosen such that they contain a relatively homogenous area (Fig. 3.5). The CNR for each patch was given by:

$$CNR_{patch,i} = \frac{\mu_{patch,i} - \mu_{sample\,body}}{\sigma_{background}} \tag{3.2}$$
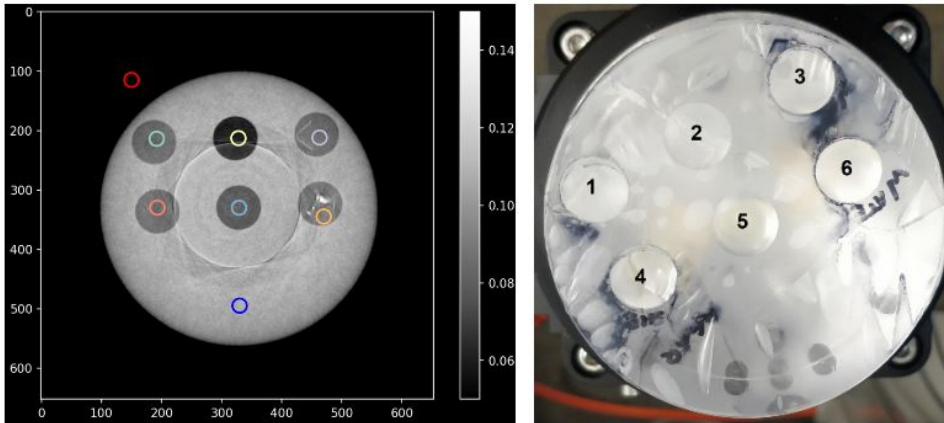
Figure 3.5: Patches used to calculate the CNRs. Left: the patches displayed on a phase image of the phantom. The blue patch below the cluster of 6 patches was used to find the average for the sample body, and the red patch on the top left of the phantom was used to find the standard deviation of the background noisy region. Right: The phantom with the corresponding patches labeled 1 through 6.

19

Patch no.	D—0.2 RPM	C—0.2 RPM	D—1 RPM	C—1 RPM
1	2.34	2.52	2.97	1.49
2	2.57	2.16	4.46	3.65
3	5.31	4.57	5.91	5.21
4	12.47	14.56	16.99	15.44
5	5.21	6.60	10.24	6.35
6	6.45	5.15	7.62	5.48

Table 3.1: CNRs calculated for phase contrast images recorded with four acquisition modes. 'C' and 'D' denote continuous and discrete phase stepping respectively.

3.4 Discussion

It should be noted that the images acquired using continuous phase stepping had an intrinsic blur. This was because during the binning process for each phase step, frames would be binned that were recorded over a range of G0 positions. This is unlike discrete phase stepping, where the frames binned were recorded for a fixed G0 position. Additionally, using the entire wavetable - including the acceleration and deceleration of G0 - meant that there was oversampling at the start and end of the wavetable relative to the linear, more uniform region. This is addressed in Chapter 4.

The CNRs (Table 3.1) for tomographic imaging at the low rotation speed of 0.2 RPM are similar for discrete and continuous phase stepping. This can be explained by the fact that due to the slower rotation, data can be acquired for a greater duration for each angular projection relative to a faster rotation speed.

For fast rotation at 1 RPM, discrete phase stepping outperforms continuous phase stepping (see Table 3.1) for every patch. Patches 1 and 5 are noteworthy as discrete phase stepping outperforms continuous by significant amounts (2.97 vs 1.48 and 10.24 vs 6.35 respectively). For 0.2 RPM, continuous stepping outperforms discrete stepping for these same patches as well as for patches 1 and 4, which indicates that continuous phase stepping can improve results for slow rotation speeds.

Chapter 4

Piezo Control for Continuous Phase Stepping

As mentioned in Chapter 3, G0 is moved perpendicular to the beam direction in order to achieve phase stepping. This is done using a piezo motor, which operates based on a principle called the piezoelectric effect; a piezoelectric material expands and contracts depending on the electric voltage applied across it.

In the computed tomography image acquisition in Chapter 3, the accelerating and decelerating nature of the piezo driver's wavetable (Fig. 2.2) meant that there was oversampling towards the beginning and end of G0's movement profile. In order to ensure uniform sampling, it was necessary to acquire the image only during the linear region of the wavetable. There were two components to this: finding G0's position for each frame and selecting the linear region G0's movement profile. After this, an acquisition protocol could be written that would acquire frames over a linear span matching a desired period of G0.

4.1 Matching frames to G0's position

The function that controls the piezo driver to move G0 contained a loop that recorded the piezo's position and its respective time. Before this loop, an array was created that contained the desired frame times. In this array, the interval between each entry equaled the time for each frame's acquisition. In order to match the desired frame time to the piezo's time, a threshold was used when comparing the piezo time and the desired frame time. The difference between the piezo time and the frame time needed to be under this threshold for G0's location and time to be stored. The threshold was on the scale of below 4 ms and scaled linearly as the imaging duration increased. This was done to minimize computational memory usage over

longer wavetable durations and to ensure complete recording of the piezo positions and times.
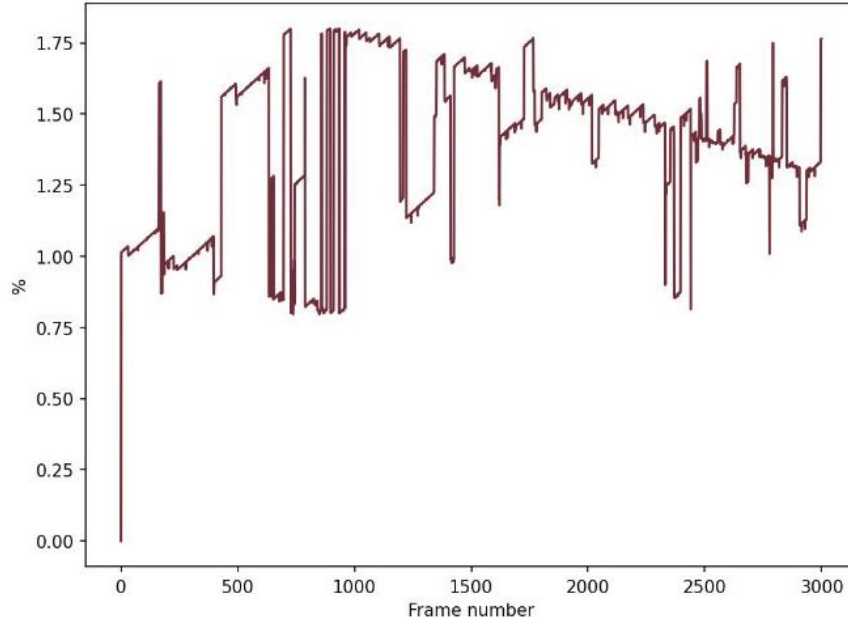
Figure 4.1: The discrepancy between the recorded G0 times and the ideal frame times, displayed as a percentage of the single frame duration. This plot corresponds to an imaging duration of 300s.

4.2 Finding the linear region of G0's movement profile

After matching G0's position to the frames, the linear region of the wavetable needed to be extracted. This was done in two steps: fitting G0's positions and the respective times with a polynomial and examining the second derivative of this fit to select the linear region. The first step was achieved by using the function *polyfit* that is in the *numpy* library on Python [6]. The degree chosen was 15 as this was the highest degree for which overfitting did not occur. For the second step, the threshold for the second derivative with respect to time scaled with the inverse of the imaging time. To find the time at which the linear region started, the array with the second derivatives was iterated through. For a point to be classified as linear, the absolute value of each point as well as the mean of the absolute values of the next five points needed to be under the threshold. The same was done for finding the point when the linearity stops, but with backward iteration through the second derivative values rather than forward.

Once the start and end locations for which G0's movement was linear were

found, the span of the linear region could be calculated. Signal retrieval could then be performed on the flat field measurement's frames that corresponded to the linear region. This retrieval would yield the period of G0. By iterating through the array containing G0's position for each frame, one could find the duration at which the distance linearly moved equaled the calculated period. The quality of the polynomial fit was better if more data was available. Therefore, in order to find the ideal table point at which linearity started (further explained in Section 4.3), a wavetable executed for a duration of 600 s was used.
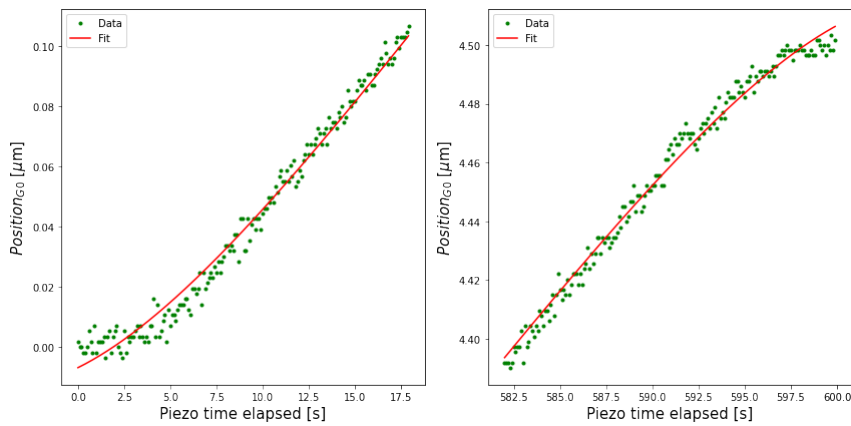
Figure 4.2: The raw G0 positions plotted with the polynomial fit for an imaging duration of 300s. Left: at the start of the wavetable. Right: towards the end of the wavetable.

23
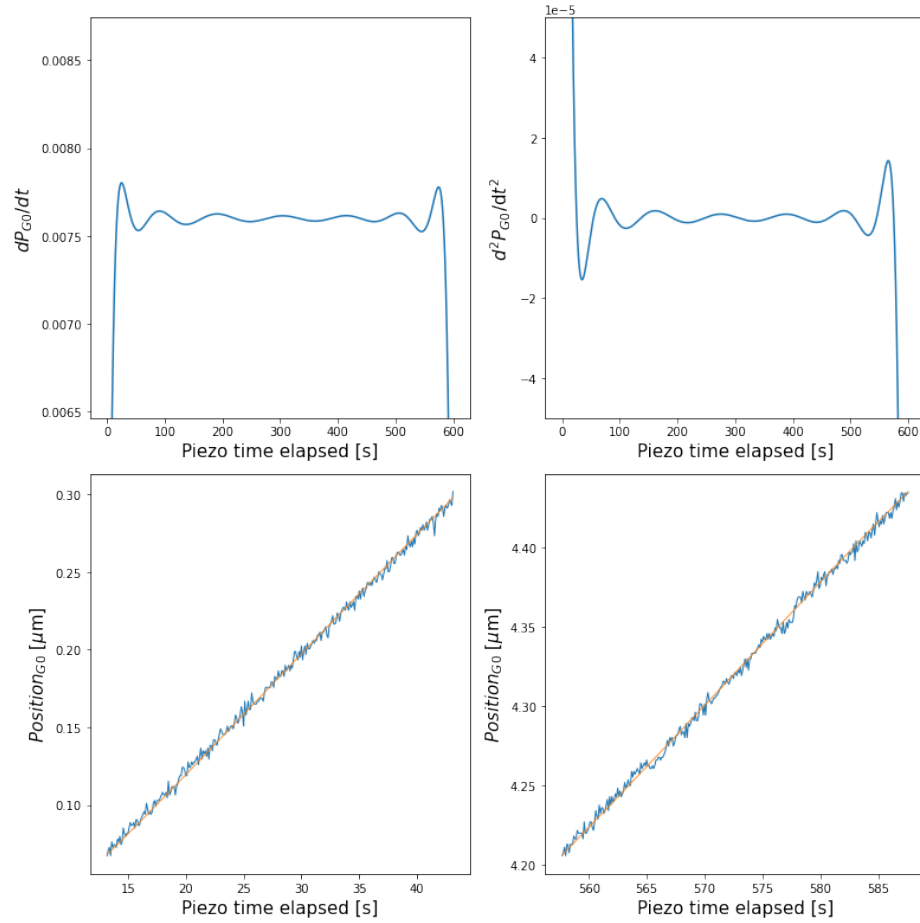
Figure 4.3: Top left: the first derivative of the polynomial fit. From t = 75 s to 550 s, the value here is constant (with negligible deviations) and nonzero, which indicates linearity. Top right: the second derivative of the polynomial fit. From t = 75 s to 550 s, the value here is zero (with negligible deviations), which indicates linearity. Bottom left: the raw data and fit at the start of the linear region. Bottom right: raw data and fit towards the end of the linear region.

Figure 4.4: The entirety of G0's recorded positions and times, along with the linear region. The blue point represents the table point at which linearity begins.

4.3 Implementing acquisition for a desired G0 period

In order to generalize this process for different imaging durations, the number of table points in the wavetable and the servo update time were used. With these values, one could calculate the table rate, which gives the number of servo-loop cycles to be used for each table point [4] The table rate could be calculated as follows [4]:

$$Table\ rate = \frac{Wavetable\ duration}{N_{table\ points} \times Time_{servo\ update}} \tag{4.1}$$

In order to find the table point at which G0's movement starts to be linear, the time at which linearity started was used. Eq 4.1 can be rearranged to give:

$$N_{linearity,start} = \frac{Time_{linearity,start}}{Table\ rate \times Time_{servo\ update}} \tag{4.2}$$

Eq. 4.2 could also be used to find the table point N_{period} corresponding to the location where G0 had moved by one period in a linear manner. The goal of converting the times to table points was to find an acquisition protocol that operates independent of the imaging duration. The image should be

acquired when G0 is within the interval of these table points. Knowing the desired table points and the imaging duration, one could find a new table rate:

$$Table\ rate = \frac{Imaging\ duration}{(N_{period} - N_{linearity,start}) \times Time_{servo\ update}} \quad (4.3)$$

The wavetable duration calculated must ensure that the linear motion spanning G0's calculated period occurs over a time interval equaling the imaging duration. By plugging the acquisition table rate from Eq. 4.3 into Eq. 4.1, this wavetable duration could be calculated:

$$Wavetable\ duration_{acq} = \frac{N_{table\ points}}{(N_{period} - N_{linearity,start})} \times Imaging\ duration \quad (4.4)$$

In order for the data acquisition to start at the right time, a time interval between the initialization of the wavetable and the start of acquisition was necessary. This time interval was given by:

$$Wait\ time = \frac{N_{linearity,start}}{N_{table\ points}} \times Wavetable\ duration_{acq} \quad (4.5)$$

Using the approach detailed above, an imaging acquisition protocol was implemented that could acquire frames over the span of a chosen period for any given imaging time. This was tested by measuring two flat field images for different imaging durations and comparing their phase images.
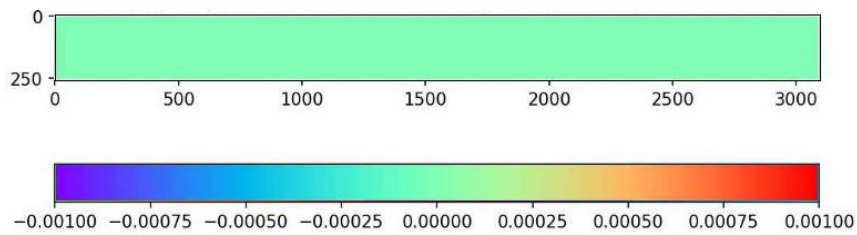
Figure 4.5: The difference in phase between flat field images acquired for imaging durations of 30s and 120s.

4.4 Discussion

The matching of piezo times with frame times (Section 4.1) was successful according to Fig. 4.1. The percentage discrepancy between piezo and frame times would increase with imaging duration and frame rate. The latter was

to be expected due to the time resolving limits of the time readout program. For a higher frame rate, even if the percentage discrepancy was larger, the absolute time discrepancy was still small i.e. on the order of ¡5 ms. The reason that the percentage discrepancy increased with imaging duration had to do with how the piezo readout times and frame times were compared; the threshold used for this scaled with imaging duration while the frame rate stayed the same.

As evidenced by Fig. 4.5, the difference in phase of two flat field images with different imaging durations (30 s and 120 s) was negligible, which showed that the acquisition protocol worked as intended. The phase difference between the two durations being negligible showed that phase stepping data was collected over the same G0 range. Desired periods could therefore be imaged independently of imaging duration.

Chapter 5

G0 Period Calculation for Various Phase Stepping Methods

Continuous phase stepping can be applied to fast stepping TLI methods; this can help reduce acquisition times as well as the amount of data required for reconstructions. An example of this is the sliding window interlaced method proposed by I. Zanette *et al* [7].
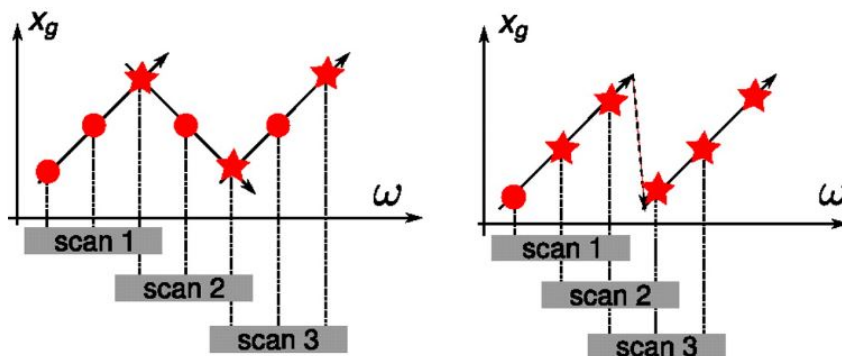
Figure 5.1: Left: stepping window zigzag method. Right: stepping window interlaced method. ω denotes the projection angle and X_g denotes the phase stepping axis. A data point being shaped as a star indicates that it can be used in more than one phase stepping curve. This image was taken from [7].

The methods shown here would entail using each reading for more than one phase stepping curve i.e. a single reading could be used to fit multiple projections [7]. In order to take a high number of angular projections, fast stepping would be required. This could potentially be done via the wavetables already detailed. However, for this to be applied to tomographic imaging, the period of G0 must be known precisely for every position of G0.

5.1 Period calculation for continuous phase stepping

Periods were calculated from flat field measurements using signal retrieval. Five flat images were acquired for exposure times ranging from 10 to 300 s and the respective periods were stored.

For continuous phase stepping, wavetables 1 and 2 were used; these had an amplitude of 4.51 μm and 20 μm respectively. The frames that were acquired during the linear region of the wavetable were selected, and the distance traveled by G0 over this region were recorded. The frames were then binned into distance intervals of 0.82 μm. This interval was chosen as it enabled 5 phase steps to be included in the linear span of wavetable 1. Wavetable 1 and 2 measurements contained 5 and 22 phase steps respectively. In the former case, the signal retrieval least squares fit yielded periods that were well below the expected value when performed over all the phase steps. So, signal retrieval was performed on the first 5 phase steps of the measurements from Wavetable 2.
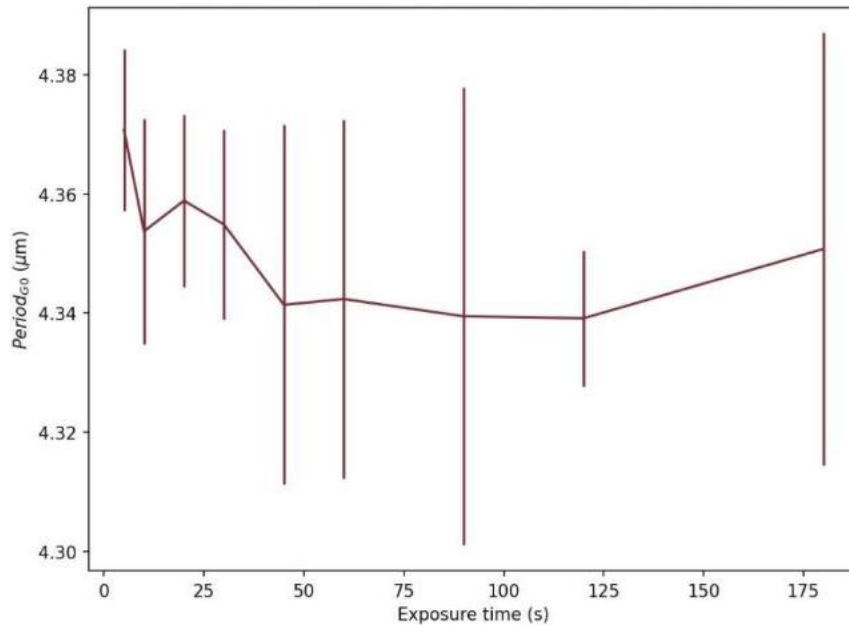
Figure 5.2: Periods calculated for different imaging durations for continuous phase stepping with wavetable 1.

Figure 5.3: Periods calculated for different imaging durations for continuous phase stepping with wavetable 2.

After averaging all the recorded periods, wavetables 1 and 2 yielded a period of $4.350 \pm 0.027 \mu m$ and $4.315 \pm 0.064 \mu m$ respectively. The reason for wavetable 3's higher standard deviation was the selecting of the first 5 phase steps. These 5 phase steps represented a smaller proportion of the exposure time than Table 5 and therefore contained less statistics.

Looking at Fig. 5.2, continuous phase stepping measurements made at low durations had a generally higher average calculated period. From a duration of 30 s and up, the average period varied less. This is due to having higher statistics i.e. more measured photons than lower durations.

5.2 Period calculation for discrete phase stepping

The process from Section 5.1 was repeated for discrete phase stepping. The step size used was the same as the binning intervals for the continuous phase stepping measurements. The distances spanned by G0 were chosen such that they were equal to the linear distances spanned by wavetables 1 and 2. Like in Section 5.1, the signal retrieval for the span matching wavetable 2 was performed on the first 5 phase steps.
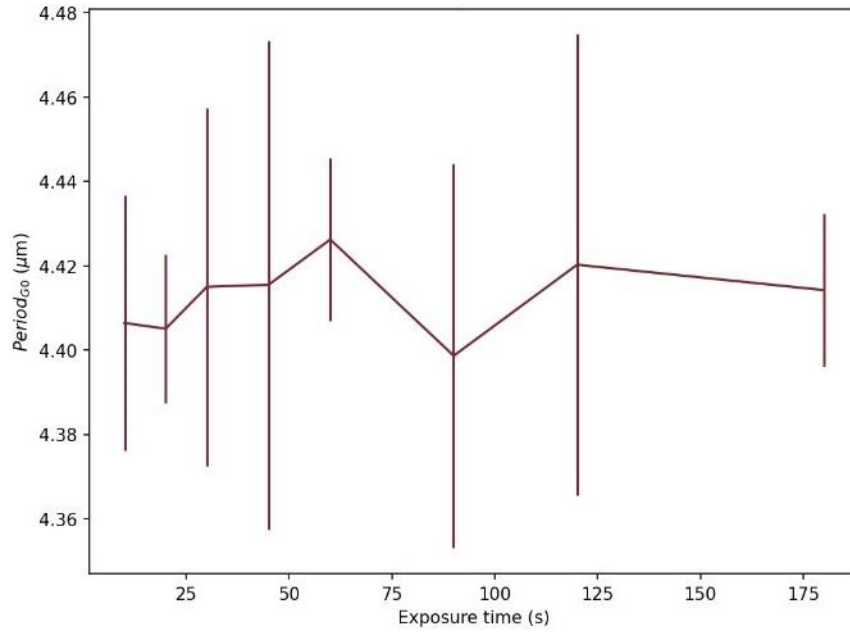
Figure 5.4: Periods calculated for different imaging durations for discrete phase stepping matching the linear span of wavetable 1.
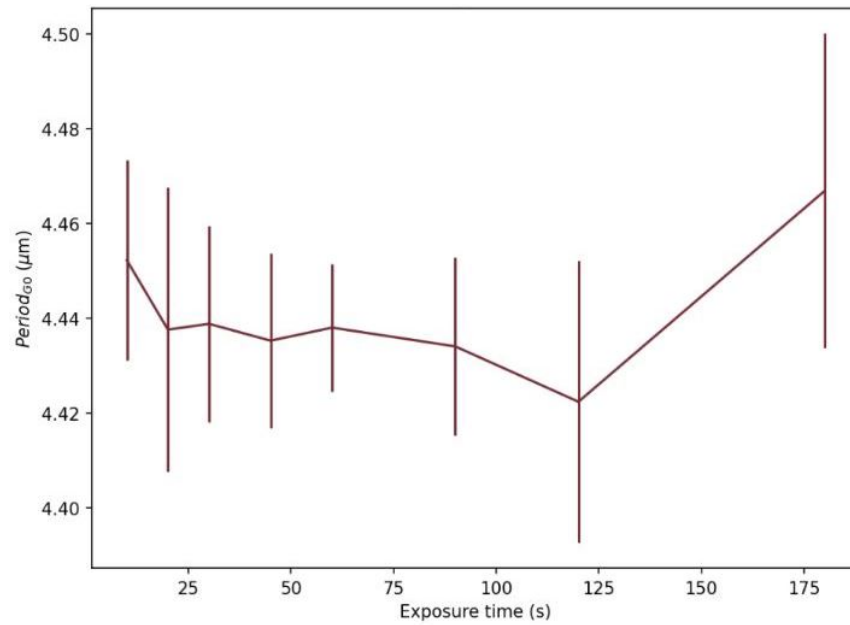
Figure 5.5: Periods calculated for different imaging durations for discrete phase stepping matching the linear span of wavetable 2.

The discrete phase stepping measurements matching the linear spans of wavetables 1 and 2 yielded periods of $4.439 \pm 0.027 \mu m$ and $4.413 \pm 0.040 \mu m$. Unlike for the continuous stepping measurements, the average periods calculated from lower imaging durations were not noticeably greater than longer durations for discrete phase stepping.

5.3 Calculating periods for different starting phase steps

Because the signal retrieval for the longer span (wavetable 2) was performed on only the first 5 phase steps out of 22, it was necessary to see whether choosing a different set of 5 phase steps would yield the same period. The signal retrieval was performed for different windows of 5 phase steps each. This was done for continuous and discrete phase stepping. The step sizes were kept constant and matched to the binning distance interval for wavetable 2.
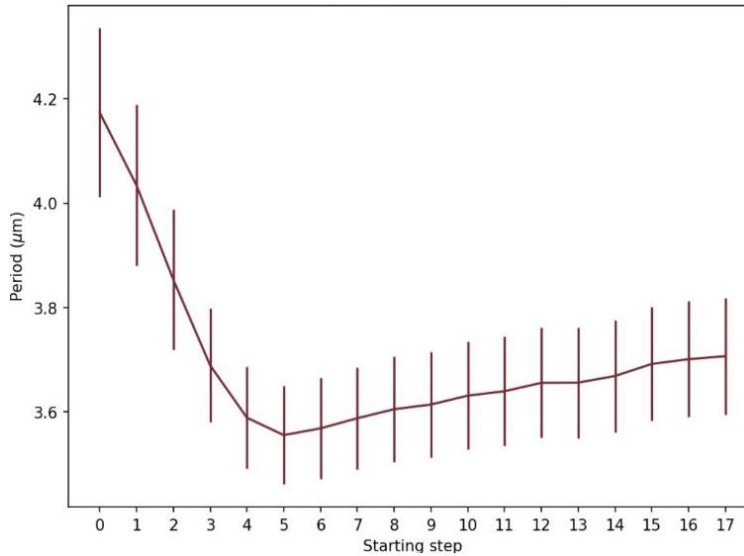
Figure 5.6: Calculated periods and starting steps for continuous phase stepping with wavetable 2.

As shown by Fig. 5.6, the periods calculated for continuous phase stepping were dependent on the phase step that was chosen as the start of the window. This needed to be tested with discrete phase stepping in order to show that the result was consistent with continuous phase stepping. This was done for two spans: one that matched the linear region for wavetable 2 and one that was significantly greater. The latter contained 88 phase steps and spanned 72.16 μm.
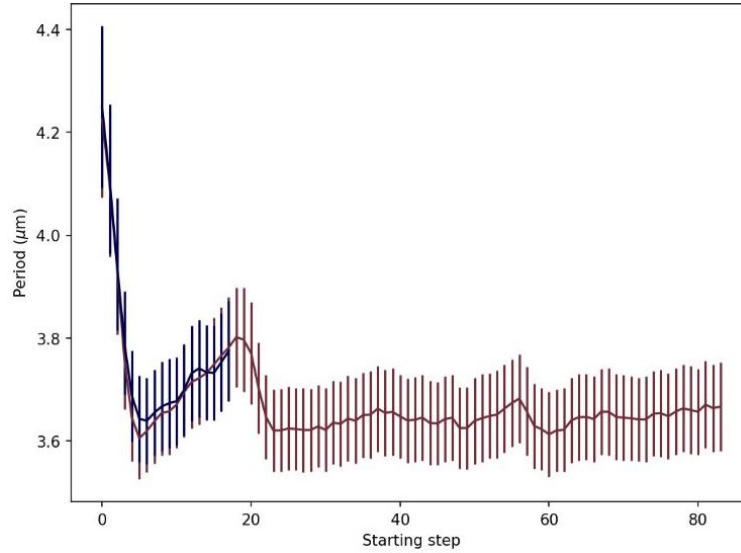
Figure 5.7: Calculated periods and starting steps for discrete phase stepping with the same step size as wavetable 2. In red: calculations for 88 phase steps. In blue: calculations for the discrete stepping measurement with the same span as the linear region of wavetable 2.

5.4 Discussion

The mean periods for the first 5 phase steps discrete phase stepping (Section 5.2) were generally greater than in the continuous case (Section 5.1). For discrete stepping, the means for both spans were above 4.4 μm, whereas for continuous stepping the means were closer to 4.3 μm. The discrepancy relative to continuous measurements was 0.089 and 0.098 μm for wavetables 1 and 2 respectively. All of these periods are generally close to the expected G0 period of 4.2 μm, although continuous phase stepping yields a result that is closer.

In Section 5.3, the discrete phase stepping measurements' calculated periods showed the same behaviour as the continuous measurement. Because this was repeatable, the results must be a system property. Other than the window with a starting step of 0, the other windows yielded periods that were significantly lower than the expected G0 period of 4.2 μm. The measurement over a larger span also showed low periods. However, the periods seem to stabilize after a starting step of 20. This information is potentially useful if fast phase stepping is desired; the period at different G0 positions could be used for calibration for an application such as interlaced stepping [7].

Chapter 6

Conclusion

Continuous phase stepping was shown to be a valid way of acquiring phase stepping data (Section 3.3). For slow rotations (0.2 RPM), its CNRs were comparable with discrete stepping, but it was outperformed by discrete stepping for higher rotation speeds (1 RPM). DPC values reconstructed from the tomographic images show that the method yielded valid results, as these values were similar for discrete and continuous phase stepping. To improve on comparisons between the two methods, one could measure the total imaging duration which would include the time taken for stepping and translation of the sample for flat-field measurements. If continuous phase stepping can be done in a shorter total duration with similar image quality, then this would help the group at PSI to save time during data acquisition. Certain applications, such as helical scanning, cannot afford to have dead time while G0 is discretely stepped, but continuous phase stepping would be well suited to such an application.

The imaging protocol to acquire data over a desired period for continuous phase stepping was implemented successfully. This protocol sought to perform such imaging in a manner that was general with regards to imaging duration and it did so successfully (Fig. 4.5). Additionally, a pipeline for piezo position readout corresponding to each acquired image frame was integrated in the system control scripts (Fig. 4.1).

It was found that the period of the phase stepping curve was dependent on the grating's position. This knowledge can be applied as a calibration metric to a future implementation of fast stepping methods such as interlaced stepping [7]. The wavetables could be executed in a manner which runs consecutive linear profiles with added offsets. This could help achieve interlaced stepping [7]. A next step could be to develop a scheme that implements this and couple it with the knowledge of the G0's position-dependent periodicity to organise frames into phase steps based on their G0 position.

Bibliography

[1] Andreas Maier, Stefan Steidl, Vincent Christlein, and Joachim Hornegger. *Medical Imaging System, An Introductory Guide*. Springer Open, 2018.

[2] J.H. Hubbel and S.M. Seltzer. Tables of x-ray mass attenuation coefficients and mass energy-absorption coefficients from 1 kev to 20 mev for elements z = 1 to 92 and 48 additional substances of dosimetric interest, 2004.

[3] Physik Instrumente (PI) GmbH Co. KG. Pipython v. 2.8.0.3, 2022.

[4] Physik Instrumente (PI) GmbH Co. KG. Pz222e user manual e-709 digital piezo controller, 2019.

[5] ASTRA Developers. Astra toolbox documentation, 2022.

[6] NumPy Developers. Numpy v. 1.22 user guide, 2022.

[7] I. Zanette, M. Bech, and A. Rack et al. Trimodal low-dose x-ray tomography. *Proceedings of the National Academy of Sciences of the United States of America*, 109(26), 2012.